Welahettige, P. K. W., Lie, B. & Vågsæther, K. (2019). Computational Fluid Dynamics Study of Shear Thinning Fluid (Drilling Fluid) Viscosity Models in an Open Venturi Channel. *International Journal of Petroleum Science and Technology, 13*(1), 9-20.

Computational Fluid Dynamics Study of Shear Thinning Fluid (Drilling Fluid) Viscosity Models in an Open Venturi Channel

Prasanna Welahettige, Bernt Lie, Knut Vaagsaether
Faculty of Technology,
University College of Southeast Norway,
Porsgrunn, Norway
knut.vagsather@usn.no

Abstract — We aim to develop an improved kick/loss detection technology by developing smart flow-sensor technology for returned flow from the oil well in open Venturi channels. This is a detailed study about a capacity of use of non-Newtonian fluid models in open Venturi channels. A water-based drilling fluid was used for the experiments. According to the rheometer results, at low shear rates, the fluid behaves as a pseudoplastic fluid, and at high shear rates, the fluid shows Newtonian properties. The experimental drilling fluid can be modelled with the power-law (PL) model, the Herschel-Bulkley (HB) model, the Carreau viscosity model, and the Cross viscosity model. Experimental flow depth measurements in an open Venturi channel were used to validate the simulation results. For the complete open channel, the strain rate range was 0.02 to 2100 1/s. The highest strain rate was on the walls of the channel, with 2100 1/s, while the fluid near to the free surface had a strain rate range of 0.02 to 200 1/s. All non-Newtonian models mentioned above can be used for the drilling fluid at a shear rate range of 0 to 2100 1/s in open Venturi channel flows. Even though different non-Newtonian models predict different wall shear stresses, these differences do not significantly affect the open channel flow depth and velocity values.

Keywords — Drilling fluid, shear thinning, non-Newtonian, viscosity, models, CFD

1 Introduction

Operating conditions for drill operation may cause various problems: if the downhole pressure is too high, the drilling mud may force drill cuttings and oil into the reservoir formation ("loss"), thus reducing the permeability at later production. On the other hand, if the downhole pressure is too low, it may allow for the premature flow of oil from the reservoir into the drill string. For safe drill operation, it is critical to detect the occurrence of "kick" and "loss". In principle, "kick" and "loss" may be detected if there is a difference in drill oil returned from the drill string compared to what is pumped down.

We intend to improve kick/loss detection by developing smart flow-sensor technology for returned fluid flow from the drilling well in open Venturi channels. On-line model development needs to have a good understanding of the behavior of the drilling fluids. This is a detailed study of non-Newtonian fluid models, and the effect of their parameters on flow depth and velocity. Even though computational fluid dynamics (CFD) simulation of drilling fluid flow in pipes is available in the literature, there are few cases of 3-D CFD drilling flow analysis in open Venturi channels: this research gap is attempted to be addressed with this study. One of the advantages of using a Venturi region is that it can generate both subcritical and supercritical flows, respectively, before and after the Venturi region for the same flow rate.

2 Non-Newtonian friction models

Viscous force can be considered a surface force, and it is a function of the local deformation rate or strain rate. Local deformation consists of linear elongation deformation and linear shearing deformation. The power-law (PL) model, $n < 1$, can be considered as a shear-thinning model [1].

$$\eta = k\dot{\gamma}^{n-1}. \tag{1}$$

The Herschel-Bulkley model combines the properties of Bingham and power-law fluids. When, $n < 1$, the Herschel-Bulkley model can be considered as a shear-thinning fluid model [2–4]. The yield stress τ_y is the shear stress at zero shear rate.

$$\eta = \frac{\tau_y}{\dot{\gamma}} + k\dot{\gamma}^{n-1} \tag{2}$$

The Carreau viscosity model gives a solution for the significant deviations of the power-law model at very high and very low shear rates. At low shear rates, $\dot{\gamma} \ll 1/\lambda$, the Carreau model acts like the Newtonian law model, and at high shear rates, $\dot{\gamma} \gg 1/\lambda$, it acts like the power-law model [4–6]. For the shear-thinning fluid, the viscosity reduces from η_0 to η_∞ when the shear rate is increased.

$$\eta = \eta_\infty + (\eta_0 - \eta_\infty)(1 + (\lambda\dot{\gamma})^2)^{\frac{n-1}{2}} \tag{3}$$

In the Cross model [7], the relaxation time λ is the controlling parameter.

$$\eta = \eta_\infty + \frac{(\eta_0 - \eta_\infty)}{(1 + (\lambda\dot{\gamma})^{1-n})} \tag{4}$$

3 CFD model

The ANSYS Fluent 16.2 commercial tool is used for the simulations. The primary and secondary phases are air and non-Newtonian fluid, respectively, in the multiphase volume of fluid (VOF) model. The standard k-ε model[8] was used as the turbulence model, and the semi-implicit method for the pressure linked equations (SIMPLE) scheme was used for the pressure-velocity decoupling. The non-Newtonian properties were fed by changing the viscosity model parameters of the fluid. Equations (1)-(4) are used for viscosity calculation for each non-Newtonian model. Non-Newtonian viscosity is considered to be a function of the shear rate in ANSYS Fluent [9]. The interface is considered a shape interface. Grid fineness gives a sharp interface between air and liquid [10]. A constant flow rate was given at the inlet, which was 400 kg/min for drilling fluid and zero for the air in x-direction. The bottom and the sidewalls were considered stationary walls at no-slip shear conditions. The wall roughness height was 15 µm [10]. In a previous study [10], mesh dependence was analyzed, and the same mesh was used in this study as well . The mesh used in the simulation contains 0.37 million elements with a maximum cell face size 10 mm and minimum cell face size 0.54 mm, see Figure 1.

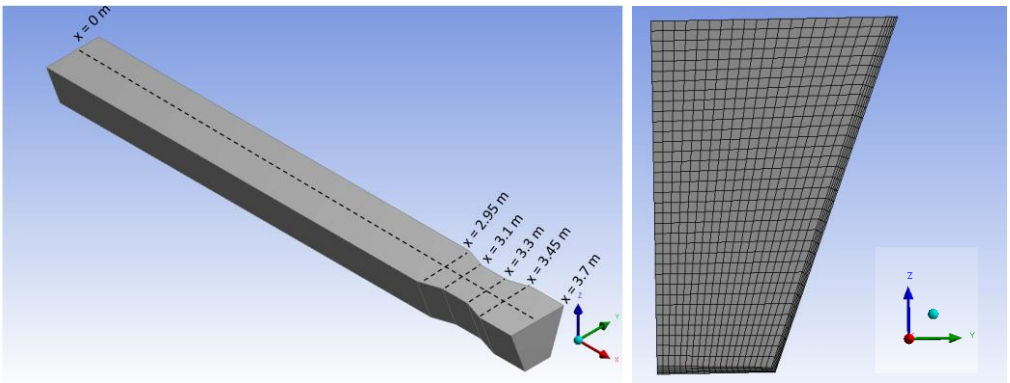

Figure 1. The channel used in the simulation is drawn similar with the channel used in experiment. The shape of the channel is trapezoidal and contains a Venturi section. The left side shows half of the cross-section of the mesh.

4 Viscosity and density measurements fit non-Newtonian models

A water-based drilling fluid was used for the experiments; it contained Potassium carbonate, Xanthan gum, and water. An Anton Paar MCR 101 viscosity meter was used for viscosity measurements. The minimum shear rate, it is able to give, is 100 1/s, less than this value produce large error in viscosity measuring. The effect of shear rates below 100 1/s is studied with simulation results. At lower shear rates, the fluid behaves as a pseudoplastic fluid. As the shear rate increases, the fluid gradually shows Newtonian properties. The rheology of the xanthan gum solution is matched with Rodd et al. [11] and Zhong et al.[12] studies. The density of the fluid is 1340 kg/m^3 at room temperature and assumed to be constant at room temperature. The density of drilling fluid was measured using Anton Paar DMA 4500: The density of the fluid is 1340 kg/m^3 at room temperature and assumed to be constant at room temperature.

The viscosity of shear-thinning fluids decreases from η_0 to η_∞, when the shear rate is increased [4]. For shear-thinning fluids $n < 1$: the curve fitting was done by fitting model parameters to the experimental viscosity values against the shear rate. The curve-fitted parameters for Equations (1)-(4) are shown in Table 1. Figure 2 shows viscosity vs. shear rate for the non-Newtonian models. The models' parameters are based on the curve-fitted values from Table 1.

Table 1. The curve-fitted parameters for non-Newtonian fluid models based on the rheometer experimental results.

	k	n	τ_y	λ	η_0	η_∞
PL	0.0390	0.7402	-	-	-	-
HB	0.0281	0.7882	0.1	-	-	-
Carreau	-	0.6443	-	0.0095	0.01384	0.00032
Cross	-	0.04	-	0.0021	0.0142	0.00247
Newtonian	0.01	1	-	-	-	-

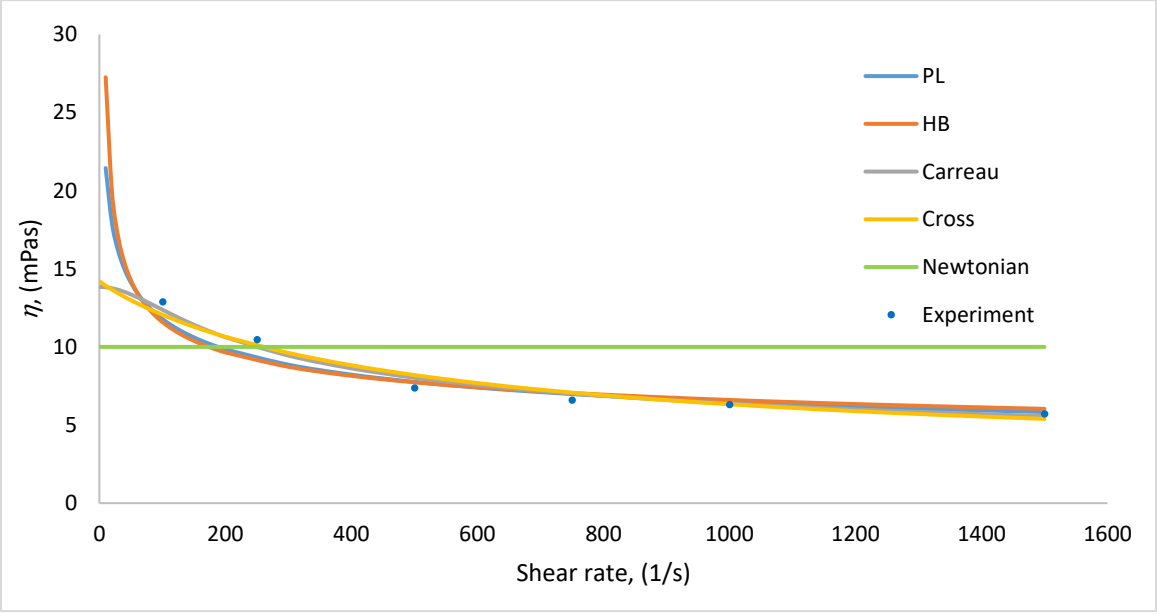

Figure 2. Shear stress vs. viscosity curves for non-Newtonian models. The model parameters are from Table 1. Experimental results are from the rheometer.

5 Experimental setup

The open Venturi channel used in the experiment contains level sensors, those can movable along the channel central axis (see Figure 3). Flow loop of the rig contains: an open Venturi channel, a mud return tank, a mud pump, and a buffer tank. The ultrasonic level transmitters' readings and the Coriolis mass flow meter's reading are used in this study to evaluate the model results. The channel can be tilted, and two tilted angles are used in this study.

Figure 3. The Venturi rig located at University of South-Eastern Norway.

6 Results

In this section, simulation results are validated by comparing them with experimental results. The effects of the non-Newtonian model parameters are discussed in section 7.

6.1 Comparison of non-Newtonian viscosity models with experimental results

The simulated models' results are compared with the experimental results as shown in Figure 4 and Figure 5. Flow-depth variations along the central channel axis are compared for the channel at a horizontal angle and for the channel at -0.7 ° downward. Both results are steady state, although the channel with a gravity angle has a hydraulic jump at quasi-steady state. A similar hydraulic jump was observed for water in our previous study [13].

With the channel at a horizontal angle, simulation and experimental results are well matched. All the non-Newtonian fluid models give almost equal results. With the channel at a -0.7° angle downward, the simulations show considerable variation before the Venturi contraction. This variation is due to the very unstable hydraulic jump in the channel; the hydraulic jump can oscillate 100 mm to the backward and upward [13]. In the simulated results, the hydraulic jump is symmetric along the channel width (along with the y-axis). However, it is non-symmetric in reality. This is also a reason for having a difference in flow depth. All the models give the same results after the Venturi expansion. Assumedly, all the models show similar results, because the fluid does not have strong non-Newtonian properties. The results might show more variation, if the drilling fluid had high viscous properties. Due to the unstable motion of the quasi-steady hydraulic jump, the flow depth is varying rapidly before the Venturi contraction. However, after the Venturi expansion, flow becomes supercritical-laminar. Due to this laminar flow behavior, experimental results and simulated results are well matched after the Venturi expansion. The critical depth value is 47 mm before and after the Venturi region, because of the same bottom width [13]. At the critical depth, the Froude number is equal to one [14]. We consider two points for the analysis of the results before and after the Venturi region, respectively, $x = 2.81$ m and $x = 3.61$ m. According to the critical depth value, the flow is subcritical at $x = 2.81$ m and supercritical at $x = 3.61$ m.

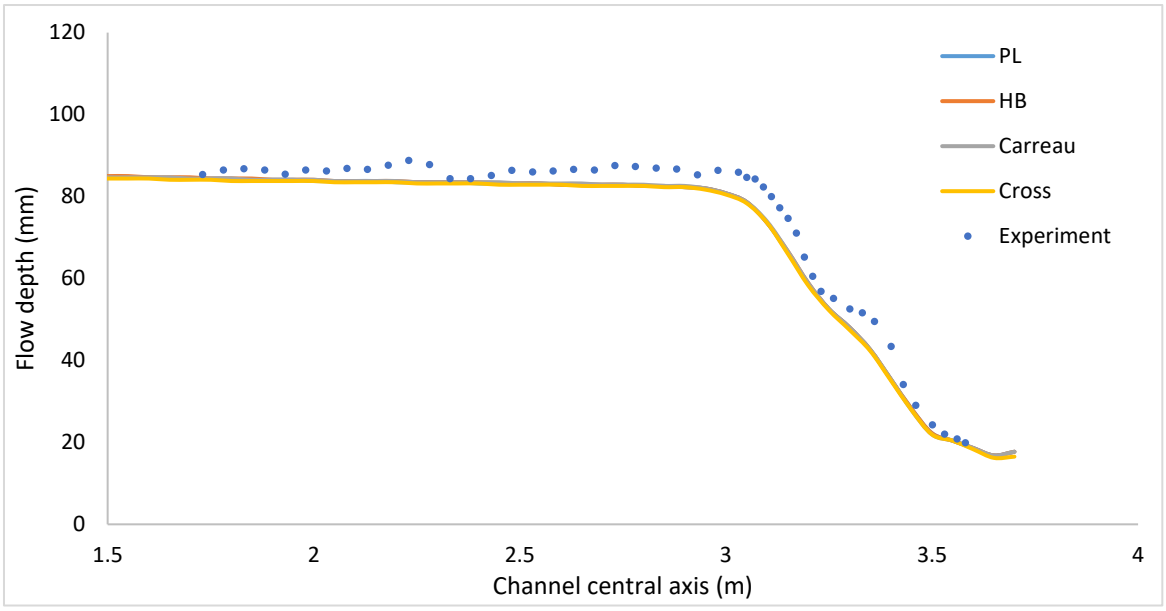

Figure 4. Flow depth along the channel axis – comparison of the viscosity models' simulated results and experimental results: The channel at a horizontal angle at steady state.

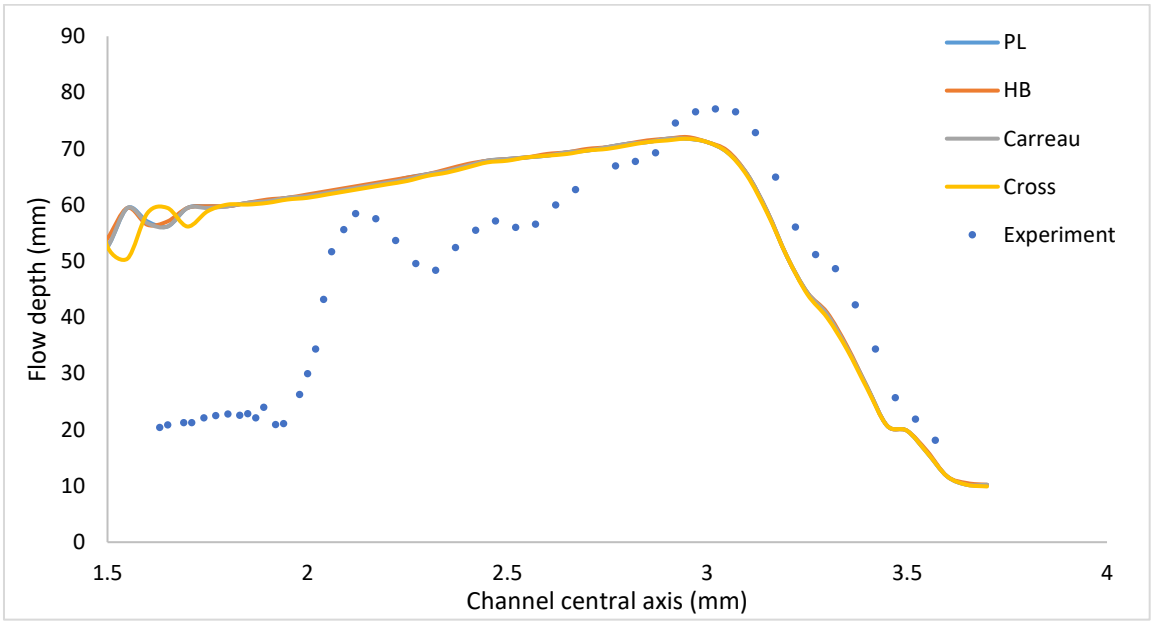

Figure 5. Flow depth along the channel axis – comparison of the viscosity models' simulated results and experimental results: (a) The channel at a horizontal angle at steady state, (b) The channel at a -0.7 º angle downward with a hydraulic jump at steady state.

7 Discussion

7.1 Velocity distributions

The simulated velocity magnitudes along the *z*-axis are shown for the non-Newtonian models before and after the Venturi region, in Figure 6 and Figure 7, respectively: Figure 6 shows the velocity profile

of subcritical flow, which is before the Venturi contraction, and Figure 7 shows the velocity profile of supercritical flow, which is after the Venturi region. At supercritical flow, the inner region disappears for a flow depth above 7 mm. After a height of 7 mm, the turbulent core becomes strong in the supercritical region. However, near to the side wall, there is a level up in supercritical flow compared to subcritical flow, see Figure 8. This might be due to the channel expansion effect, as well as a y-directional velocity reduction from the wall, which leads to the conversion of kinetic energy into potential energy. According to Longo et al. [15], another minor effect might originate from yield stress. The yield stress of this particular fluid, however, has a small value (0.1 Pa), which indicates that this effect does not play a role here. All of the non-Newtonian models give similar velocity profiles for subcritical and supercritical flows.

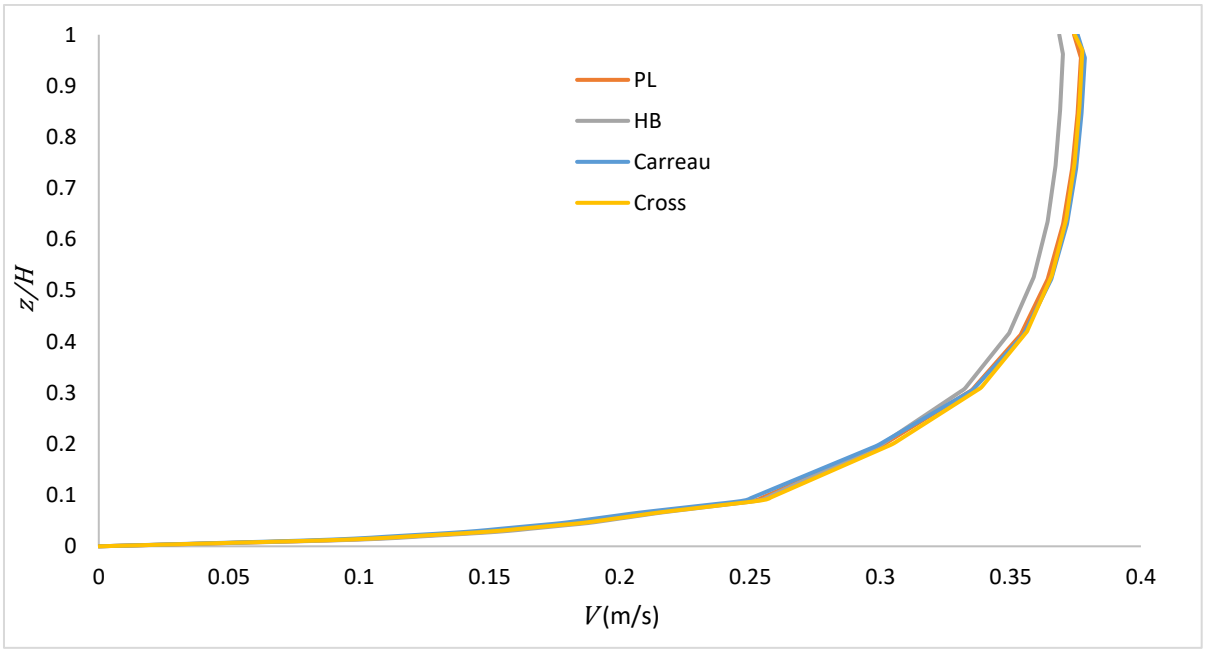

Figure 6. Vertical direction velocity profiles – comparison for non-Newtonian viscosity models at x=2.81 m, before the Venturi region.

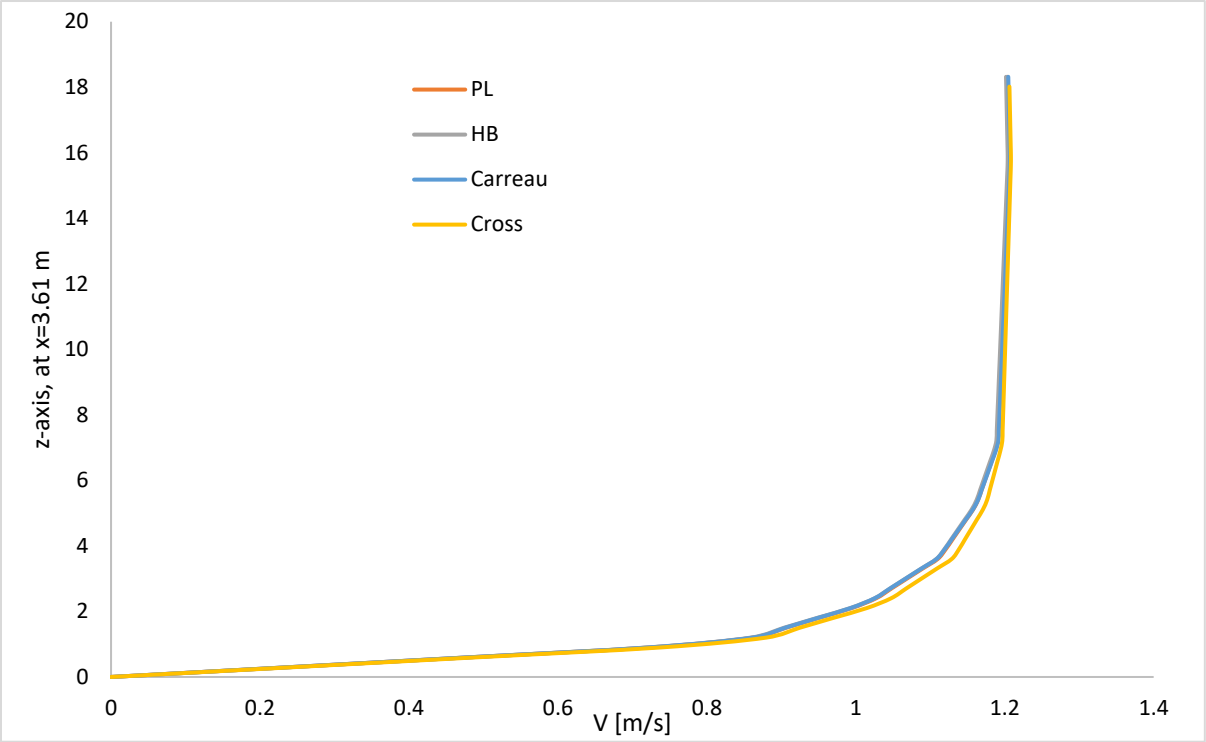

Figure 7. Vertical direction velocity profiles – comparison for non-Newtonian viscosity models at x=3.61 m, after the Venturi region.

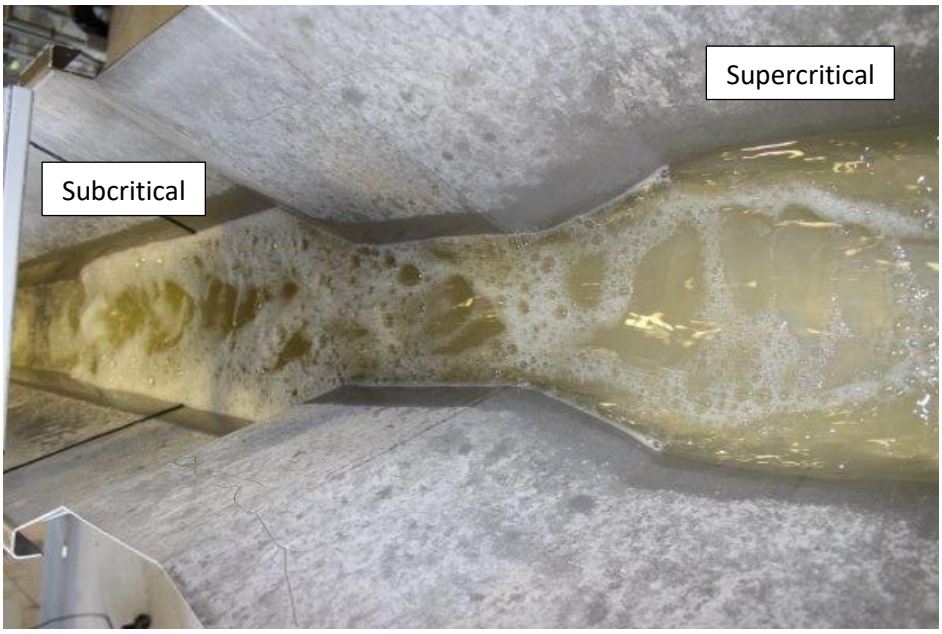

Figure 8. Experimental flow profiles before and after the Venturi region.

7.2 Simulated shear stress before and after the Venturi region

The shear stress, τ_{zx} is a function of the velocity gradient along the z-direction $\partial u/\partial z$ and the viscosity of the fluid at a given time. Figure 9 shows the shear stress τ_{zx} for subcritical, critical and supercritical flow regimes at steady state. The value of the shear stress τ_{zx}, lessens from the bottom wall to the free surface for all flow regimes: the highest wall shear stress is given by supercritical flow, which is

after the Venturi region. According to the shear stress curves, the inner region margins are at $z/H = 0.133$ and $z/H = 0.0429$ for supercritical and subcritical flow, respectively. According to Longo et al. [15], the inner shear region height for the open channel can be calculated, $z/H = 1 - \tau_0/(\rho g \sin\beta)$. By substituting, $\tau_0 \approx \tau_{zx,wall}$, we can approximate the inner region height mentioned above. The shear stress near to the free surface gives negative values with respect to the bottom shear stress direction for subcritical and critical flow. This is due to the secondary currents coming from the side walls [16,17] and is called the dip-phenomenon. Here we have noticed that the dip-phenomenon is not visible in supercritical flow.

Figure 10 shows shear stress in the x-direction perpendicular to the y-direction, τ_{yx}. Here, $y = 0$ is the center of the channel and shear stress profiles are at $z = 0.01$m above the bottom wall. The sidewall shear stress is very strong in supercritical flow compared to subcritical flow. It is also larger than the bottom wall shear stress difference of supercritical and subcritical flow. At the center of the subcritical flow, the shear stress direction is converted to the negative direction, which is due to the secondary currents as explained above. However, due to the smooth sidewalls, these secondary currents in subcritical flow are not very strong. The wall shear stress coming from the bottom wall is stronger than that coming from the sidewalls, with 12 Pa and 8 Pa, respectively.

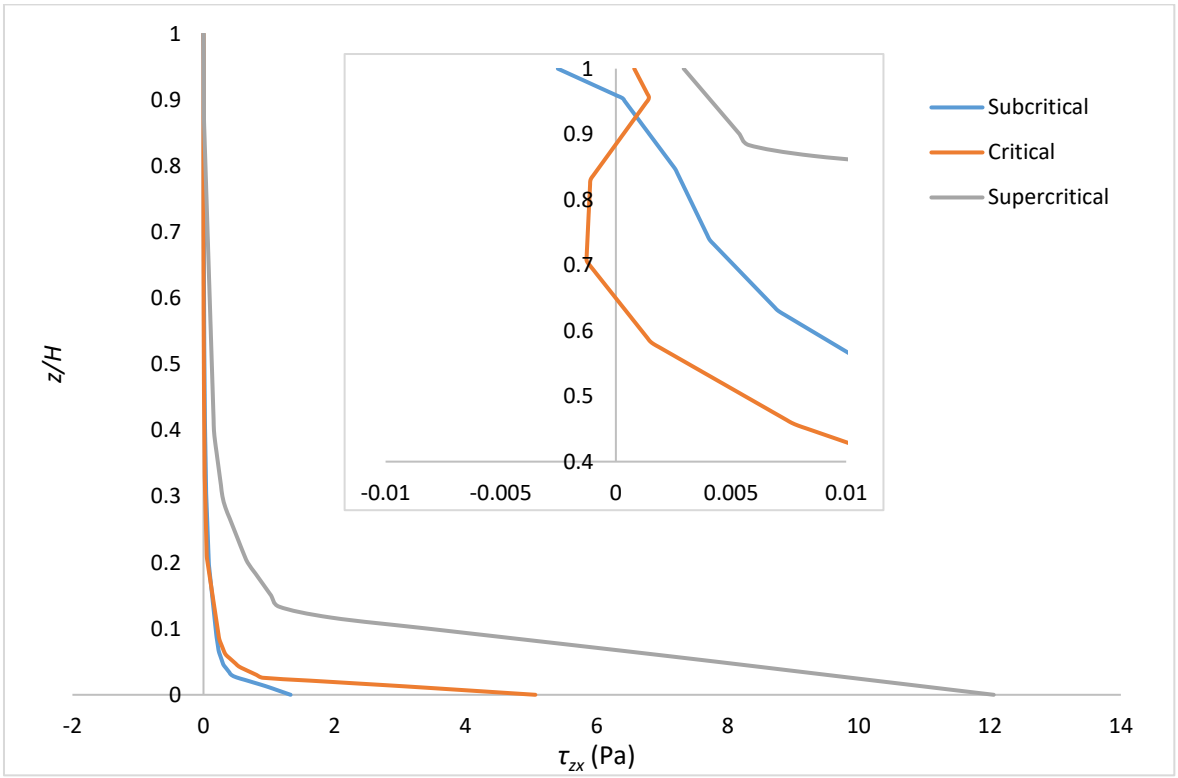

Figure 9. Shear stress in the x-direction perpendicular to the z-direction, τ_{zx}, for different flow regimes in the open Venturi channel at quasi steady state. The Carreau viscosity model was used for the viscosity calculation.

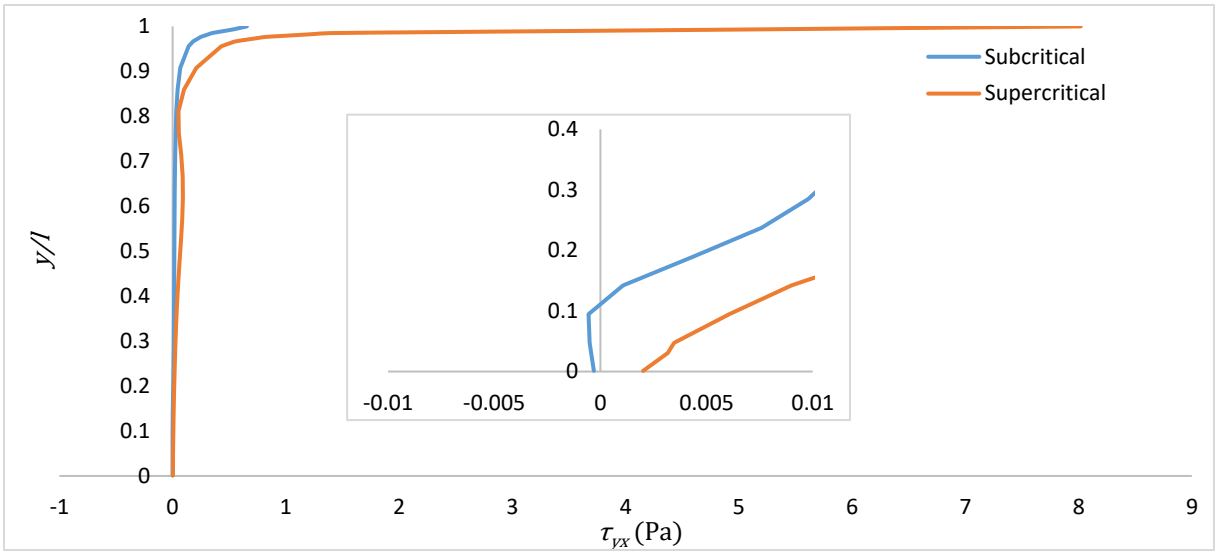

Figure 10. Shear stress in the x-direction perpendicular to the y-direction, τ_{yx}, for different flow regimes in open Venturi channel at the quasi steady state. The Carreau viscosity model was used for the viscosity calculation. Here, $z = 0.01$ m is the height from the bottom, and $l = 0.104$ m.

7.3 Shear rate at the wall

The velocity gradient at the bottom wall can have an impact on wall shear stress. Figure 11 shows the $(\partial u/\partial z)_{z=0}$ variation along the x-axis. Here, the channel is at a horizontal angle. All models give similar results except for a minor difference of the Cross model at the end of the channel. In general, the velocity gradient at the wall increases in x-direction at the bottom of the wall. This is due to the increasing velocity in the channel. The wall shear rates are also given the same values by the all the models. Therefore, these all the models can be used to simulate the model drilling fluid.

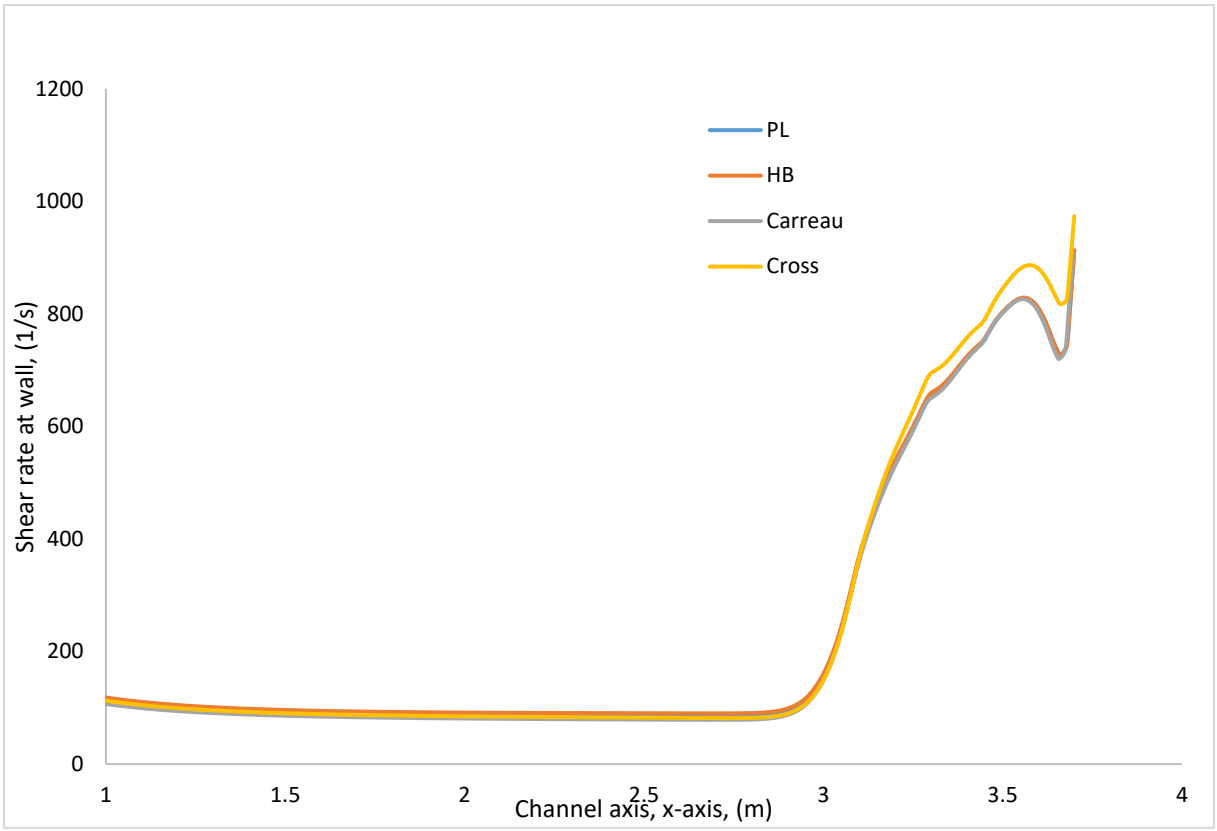

Figure 11. Shear rate at the wall along the x-axis – comparison of different non-Newtonian models

8 Conclusion

The 3-D CFD simulations were done for the experimental drilling fluid flow in an open Venturi channel. The model drilling fluid shows shear-thinning properties at lower shear rates and Newtonian properties at higher shear rates. The non-Newtonian models' results for shear-thinning fluid were validated with the experimental results. The results of all models matched well with the flow depth after the Venturi region with a quasi-steady hydraulic jump in the channel. There is a larger inner layer in subcritical flow than in supercritical flow. The velocity profiles are more fully developed after the Venturi region than before the Venturi region. The viscosity of the fluid has a greater effect on the flow depth after the Venturi contraction than before the Venturi contraction. The Xanthan gum water-based model drilling fluid in an open Venturi channel can be simulated with all of the non-Newtonian models examined in this study: the power-law model, the Herschel-Bulkley model, the Carreau viscosity model and the Cross viscosity model.

Nomenclature

H Flow depth (m)

k Fluid consistency index of the power-law model

n Flow behavior index of the power-law model

U Average velocity (m/s)

τ Shear stress (Pa)

τ_y Yield shear stress (Pa)

β Channel slope angle (degree)

$\dot{\gamma}$ Shear rate (1/s)

η Viscosity (Pa·s)

η_0 Viscosity at low rate of shear or viscosity at yield stress (Pa·s)

η_∞ Viscosity at high rate of shear (Pa·s)

λ Relaxation time (s)

Acknowledgments

We gratefully acknowledge the economic support from The Research Council of Norway and Statoil ASA through project no. 255348/E30 “Sensors and models for improved kick/loss detection in drilling (Semi-kidd)”. Sumudhu Karunarathna, Khim Chhantyal, Asanthi Jinasena, Morten Jondahl and Håkon Viumdal are acknowledged for their kind support with the experiments.

References

1. Khandelwal V, Dhiman A, Baranyi L. Laminar flow of non-Newtonian shear-thinning fluids in a T-channel. *Comput Fluids* 2015; 108: 79–91.

2. Herschel WH, Bulkley R. Measurement of consistency as applied to rubber-benzene solutions. *Proc ASTM Part II* 1926; 26: 621–629.

3. Saramito P. A new elastoviscoplastic model based on the Herschel–Bulkley viscoplastic model. *J Non-Newtonian Fluid Mech* 2009; 158: 154–161.

4. Chhabra RP, Richardson JF. *Non-Newtonian Flow and Applied Rheology : Engineering Applications.* 2nd ed. Butterworth-Heinemann, 2011.

5. Carreau PJ. Rheological Equations from Molecular Network Theories. *Trans Soc Rheol* 1972; 16: 99–127.

6. Picchi D, Poesio P, Ullmann A, et al. Characteristics of stratified flows of Newtonian/non-Newtonian shear-thinning fluids. *Int J Multiph Flow* 2017; 97: 109–133.

7. Cross MM. Relation between viscoelasticity and shear-thinning behaviour in liquids. *Rheol Acta* 1979; 18: 609–614.

8. Launder BE, Spalding DB. The numerical computation of turbulent flows. In: *Numerical Prediction of Flow, Heat Transfer, Turbulence and Combustion*. Elsevier, 1983, pp. 96–116.

9. ANSYS Fluent. *12.0 Theory Guide*. 2009.

10. Welahettige P, Lie B, Vaagsaether K. Computational fluid dynamics study of flow depth in an open Venturi channel for Newtonian fluid. In: *Proceedings of the 58th SIMS*. Reykjavik: Linköping University Electronic Press, pp. 29–34.

11. Rodd AB, Dunstan DE, Boger DV. Characterisation of xanthan gum solutions using dynamic light scattering and rheology. *Carbohydr Polym* 2000; 42: 159–174.

12. Zhong L, Oostrom M, Truex MJ, et al. Rheological behavior of xanthan gum solution related to shear thinning fluid delivery for subsurface remediation. *J Hazard Mater* 2013; 244–245: 160–170.

13. Welahettige P, Lie B, Vaagsaether K. Flow regime changes at hydraulic jumps in an open Venturi channel for Newtonian fluid. *J Comput Multiph Flows* 2017; 9(4): 169–179.

14. Akan AO. *Open channel hydraulics*. 1st ed. Elsevier/BH, 2006.

15. Longo S, Chiapponi L, Di Federico V. On the propagation of viscous gravity currents of non-Newtonian fluids in channels with varying cross section and inclination. *J Nonnewton Fluid Mech* 2016; 235: 95–108.

16. Nezu I. Open-channel flow turbulence and its research prospect in the 21st century. *J Hydraul Eng* 2005; 131: 229–246.

17. Yang S-Q, Tan S-K, Lim S-Y. Velocity distribution and dip-phenomenon in smooth uniform open channel flows. *J Hydraul Eng* 2004; 130: 1179–1186.